Implementing a multi-target-qubit controlled-NOT gate with logical qubits outside a decoherence-free subspace and its application in creating quantum entangled states

Chui-Ping Yang,[1] Qi-Ping Su,[1] Yu Zhang,[2] and Franco Nori[3,4]
[1]*Department of Physics, Hangzhou Normal University, Hangzhou, Zhejiang 311121, China*
[2]*School of Physics, Nanjing University, Nanjing 210093, China*
[3]*Theoretical Quantum Physics Laboratory, RIKEN Cluster for Pioneering Research, Wako-shi, Saitama 351-0198, Japan*
[4]*Department of Physics, University of Michigan, Ann Arbor, Michigan 48109-1040, USA*

(Received 9 January 2020; accepted 26 February 2020; published 19 March 2020)

In general, implementing a multi-logical-qubit gate by manipulating quantum states in a decoherence-free subspace (DFS) becomes more complex and difficult when increasing the number of logical qubits. In this work, we propose an idea to realize quantum gates by manipulating quantum states outside their DFS but having the states of the logical qubits remain in their DFS before and after the gate operation. This proposal has the following features: (i) because the states are manipulated outside the DFS, the multiqubit gate implementation can be simplified when compared to realizing a multiqubit gate via manipulating quantum states within the DFS, which usually requires unitary operations over a large DFS, and (ii) because the states of the logical qubits return to the DFS after the gate operation, the errors caused by decoherence during the gate operation are not accumulated for a long-running calculation, and the states of the logical qubits are immune to decoherence when they are stored. Based on this proposal, we then present a way for realizing a multi-target-qubit controlled-NOT gate using logical qubits encoded in a decoherence-free subspace against collective dephasing. This gate is realized by employing qutrits (three-level quantum systems) placed in a cavity or coupled to a resonator. This proposal has the following advantages: (i) the states of the logical qubits return to their DFS after the gate operation; (ii) the gate can be implemented with only a few basic operations; (iii) the gate operation time is independent of the number of logical qubits; (iv) this gate can be deterministically implemented because no measurement is needed; (v) the intermediate higher-energy level for all qutrits is not occupied during the entire operation, thus decoherence from this level is greatly suppressed; (vi) this proposal is universal and can be applied to realize the proposed gate using natural atoms or artificial atoms (e.g., quantum dots, nitrogen-vacancy centers, and various superconducting qutrits, etc.) placed in a cavity or coupled to a resonator. As an application, we also show how to apply this gate to create a Greenberger-Horne-Zeilinger (GHZ) entangled state of multiple logical qubits encoded in DFS, and further investigate the experimental feasibility for creating the GHZ state of three logical qubits in the DFS, by using six superconducting transmon qutrits coupled to a one-dimensional coplanar waveguide resonator.

DOI: 10.1103/PhysRevA.101.032329

I. INTRODUCTION AND MOTIVATION

Multiple qubit gates play an important role in quantum computing (QC). A multiqubit gate can in principle be constructed using basic gates such as one-qubit and two-qubit gates. However, it becomes difficult to build a multiqubit gate using basic gates because the number of basic gates increases drastically as the number of qubits increases [1–3]. Therefore, seeking efficient methods for the *direct implementation* of a multiqubit gate is an interesting and important topic.

There are two types of significant multiqubit gates, i.e., multi-control-qubit gate and multi-target-qubit gate. These two types of multiqubit gates are important in QC. For example, they have applications in quantum algorithms [4,5], quantum Fourier transform [6], and error correction [7,8]. Moreover, they have applications in quantum cloning [9] and entanglement preparation [10]. Over the past years, direct implementation of these two types of multiqubit gate has drawn much attention. The direct realization of a Toffoli gate of three physical qubits has been experimentally demonstrated in various physical systems [11–13]. In addition, based on cavity or circuit QED, many schemes have been presented for the direct realization of a multi-control-qubit gate [14–22] and a multi-target-qubit gate [23–29] with *physical qubits*.

In principle, quantum computers could solve hard computational problems much more efficiently than classical computers. However, quantum information is fragile and easily destroyed by decoherence, which is one of the main obstacles in building quantum computers. Decoherence is caused by the inevitable coupling of the computational system with its environment, which collapses the desired coherence of the system and thus degrades the efficiency of quantum computation. Hence protecting quantum information from decoherence is necessary for any quantum computing task. Among various strategies designed to protect quantum information against decoherence, decoherence-free subspaces (DFSs) open a promising way for avoiding quantum decoherence [30–32]. As is well known, the basic idea of DFSs is to utilize the symmetry structure of the coupling between the system and its environment. The experimental implementation

of DFSs in many quantum systems has already been reported [33–36].

Above, we have briefly reviewed previous works on the direct implementation of a multiqubit gate. However, it is noted that multiqubit gates based on the previous proposals [7–21] were realized with *physical qubits* instead of *logical qubits*. Because the two logic states $|0\rangle$ and $|1\rangle$ of a physical qubit do not form a DFS, the states of the physical qubits do not stay in a DFS for all three stages: (i) before the gate operation, (ii) during the gate operation, and (iii) after the gate operation. In this sense, by using the previous proposals [8–26], quantum states of qubits will undergo decoherence from all of these three stages. Also, because the states of physical qubits do not stay in a DFS, the errors caused by decoherence from each of the three stages accumulate for a long-running quantum computation. In addition, since the states of physical qubits do not stay in a DFS, decoherence from qubits is a problem during the state storage. These are some shortcomings existing in the previous proposals for implementing multiqubit gates with physical qubits.

In order to overcome decoherence, it is natural to think of implementing a multiqubit gate by encoding a physical qubit into a logical qubit with auxiliary physical qubits. However, we note that all existing DFS-based schemes only focus on, at most, one-logical-qubit gates [37–45], two-logical-qubit gates [37–47], and three-logical-qubit Toffoli gates [47]. None of the DFS proposals for directly implementing a multi-logical-qubit gate in a DFS with the number of logical qubits greater than 3 has been reported. It is commonly recognized that the procedure for implementing a multi-logical-qubit gate becomes complex when increasing the number of logical qubits. Especially, this challenge becomes more apparent when a multi-logical-qubit gate is implemented in a DFS, because unitary operations in a large DFS are required but usually hard to realize.

A. Idea for implementing quantum gates of logical qubits outside a DFS

Motivated by the above, we here propose a different idea for realizing quantum gates with logical qubits. Namely, the states of the logical qubits are manipulated *outside* the DFS during the gate operation, but remain in the DFS before and after the gate operation. This idea has the following features. (i) Because the states are manipulated outside the DFS, the multi-logical-qubit gate implementation can be simplified when compared to realizing a multi-logical-qubit gate based on manipulating quantum states within DFS, which usually requires unitary operations over a large DFS. (ii) Since the states of the logical qubits return to the DFS after the gate operation, the decoherence during the state storage (usually necessary after completing a computational task) is avoided and the errors caused by decoherence are not accumulated for a long-running quantum calculation.

B. Proposal for implementing a multi-target-qubit CNOT gate with logical qubits outside DFS

Based on the idea introduced above, in the following we will present a way to implement a multi-target-qubit controlled-NOT gate with logical qubits encoded in a DFS against collective dephasing. This gate is implemented by employing qutrits (three-level quantum systems) placed in a cavity or coupled to a resonator. In the past, much attention has been paid to quantum operations with qutrits or qudits [48–51]

As shown below, this proposal has these advantages: (i) the states of the logical qubits return to the DFS after the gate operation, (ii) the gate can be implemented with only a few basic operations, (iii) the gate operation time is independent of the number of logical qubits and thus does not increase with the number of logical qubits, (iv) this gate can be implemented in a deterministic way because no measurement on the state of the qutrits or the cavity is needed, and (v) the intermediate higher-energy level $|2\rangle$ for all qutrits is not occupied during the entire operation; thus decoherence from this level is greatly suppressed. Moreover, this proposal is universal and can be applied to realize the proposed gate using natural atoms or artificial atoms [e.g., quantum dots, nitrogen-vacancy (NV) centers, various superconducting qutrits, etc.] placed in a cavity or coupled to a resonator.

This paper is arranged as follows. In Sec. II, we briefly introduce a multi-target-qubit controlled-NOT gate with logical qubits encoded in a DFS against collective dephasing. In Sec. III, we introduce the types of interaction and the state evolutions used in the gate implementation. In Sec. IV, we show how to implement the proposed gate, by employing qutrits placed in a cavity or coupled to a resonator. In Sec. V, as an application, we show how to apply this gate to create Greenberger-Horne-Zeilinger (GHZ) entangled states of multiple logical qubits in a DFS. In Sec. VI, we further investigate the experimental feasibility for creating the GHZ state of three logical qubits in a DFS, by using six superconducting transmon qutrits coupled to a one-dimensional coplanar waveguide resonator. A brief summary is given in Sec. VII.

II. MULTI-TARGET-QUBIT CONTROLLED-NOT GATE WITH LOGICAL QUBITS ENCODED IN A DFS

We here consider n logical qubits $(1, 2, \ldots, n)$, each of which is constructed with two physical qubits. The two logical states of the logical qubit i are encoded as $|0_{L_i}\rangle = |01\rangle$ and $|1_{L_i}\rangle = |10\rangle$ $(i = 1, 2, \ldots, n)$, where the first 0 and 1 are the two logical states of the first physical qubit, while the second 0 and 1 are the two logical states of the second physical qubit. If the two physical qubits are symmetrically coupled to an environment, the two logical states $|0_{L_i}\rangle$ and $|1_{L_i}\rangle$ span a DFS protected against collective dephasing. A multi-target-qubit controlled-NOT gate (see Fig. 1), with one logical qubit (say logical qubit 1) simultaneously controlling $(n-1)$ target logical qubits (logical qubits $2, 3, \ldots,$ and n), is described by

$$\begin{aligned} |0_{L_1}\rangle|j_{L_2}\rangle|j_{L_3}\rangle\ldots|j_{L_n}\rangle &\rightarrow |0_{L_1}\rangle|j_{L_2}\rangle|j_{L_3}\rangle\ldots|j_{L_n}\rangle, \\ |1_{L_1}\rangle|j_{L_2}\rangle|j_{L_3}\rangle\ldots|j_{L_n}\rangle &\rightarrow |1_{L_1}\rangle|\bar{j}_{L_2}\rangle|\bar{j}_{L_3}\rangle\ldots|\bar{j}_{L_n}\rangle, \end{aligned} \tag{1}$$

where subscript 1 represents the control logical qubit 1, while subscripts $2, 3, \ldots, n$ represent target logical qubits $2, 3, \ldots, n$, with $\bar{j}_{L_i} = 1 - j_{L_i}$ and $j_{L_i} \in \{0, 1\}$ $(i = 2, 3, \ldots, n)$. Equation (1) implies that, when the control logical qubit is in the state $|0\rangle$, nothing happens to the states of each target logical qubit; however, when the control logical

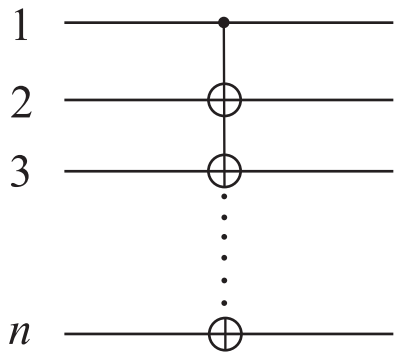

FIG. 1. Schematic circuit of a controlled-NOT gate with the control logical qubit 1 simultaneously controlling n target logical qubits $2, 3, \ldots,$ and n. The symbol $\oplus$ represents a NOT gate on each target logical qubit. If the control logical qubit 1 is in the state $|1_L\rangle$, then the state of the target logical qubit at $\oplus$ is bit flipped as $|0_L\rangle \rightarrow |1_L\rangle$ and $|1_L\rangle \rightarrow |0_L\rangle$. However, when the control logical qubit 1 is in the state $|0_L\rangle$, the state of the target logical qubit at $\oplus$ remains unchanged. Note that the two logical states of the logical qubit i are encoded as $|0_{L_i}\rangle = |01\rangle$ and $|1_{L_i}\rangle = |10\rangle$ with two physical qubits $(i = 1, 2, \ldots, n)$.

qubit is in $|1\rangle$, a bit flip happens to the state $|0\rangle$ or $|1\rangle$ of each target logic qubit.

III. TYPE OF INTERACTION AND STATE EVOLUTION

Consider now n qutrit pairs $\{1, 1'\}, \{2, 2'\}, \ldots, \{n, n'\}$ placed in a cavity or coupled to a resonator [Fig. 2(a)]. Each qutrit has three levels $|0\rangle$, $|1\rangle$, and $|2\rangle$ [Fig. 2(b) and Fig. 2(c)]. In the following, our presentation is based on qutrits with the level structure depicted in Fig. 2(b). However, it should be mentioned that the method introduced below for the gate realization applies to the qutrits having the level structure illustrated in Fig. 2(c). This is because the required Hamiltonians presented below can also be obtained for the type of level structure in Fig. 2(c).

As shown in the next sections, the gate implementation requires (i) a classical pulse resonantly interacting with the $|0\rangle \leftrightarrow |1\rangle$ transition for each of qutrit pairs $\{2, 2'\}, \{3, 3'\}, \ldots, \{n, n'\}$, (ii) the cavity resonantly interacts with the $|0\rangle \leftrightarrow |1\rangle$ transition of qutrit 1, and (iii) the cavity is dispersively coupled to the $|1\rangle \leftrightarrow |2\rangle$ transition of qutrit pairs $\{2, 2'\}, \{3, 3'\}, \ldots, \{n, n'\}$. In the following, we will give a brief introduction to the state evolution under these types of interaction.

A. Qutrit-pulse resonant interaction

Consider now a classical pulse applied to the qutrit pairs $\{2, 2'\}, \{3, 3'\}, \ldots, \{n, n'\}$. The pulse is resonant with the $|0\rangle \leftrightarrow |1\rangle$ transition of the qutrits [Fig. 3(a)]. The Hamiltonian in the interaction picture, and after making a rotating-wave approximation (RWA), is given by

$$H_1 = \Omega\, e^{-i\phi} \sum_{j=2}^{n} (|1\rangle_j\langle 0| + |1\rangle_{j'}\langle 0|) + \text{H.c.}, \tag{2}$$

where the subscript j represents qutrit j $(j = 2, 3, \ldots, n)$, subscript j' represents qutrit j' $(j' = 2', 3', \ldots, n')$, ϕ is the initial phase of the pulse, and Ω is the pulse Rabi frequency. Under this Hamiltonian, we can easily obtain the following state rotation:

$$\begin{aligned} |0\rangle &\rightarrow \cos\Omega t|0\rangle - i\, e^{-i\phi} \sin\Omega t|1\rangle, \\ |1\rangle &\rightarrow -i\, e^{i\phi} \sin\Omega t|0\rangle + \cos\Omega t|1\rangle, \end{aligned} \tag{3}$$

for each qutrit. Note that for simplicity we here consider an identical Rabi frequency for the pulse applied to each qutrit, which can be achieved by adjusting the pulse intensity.

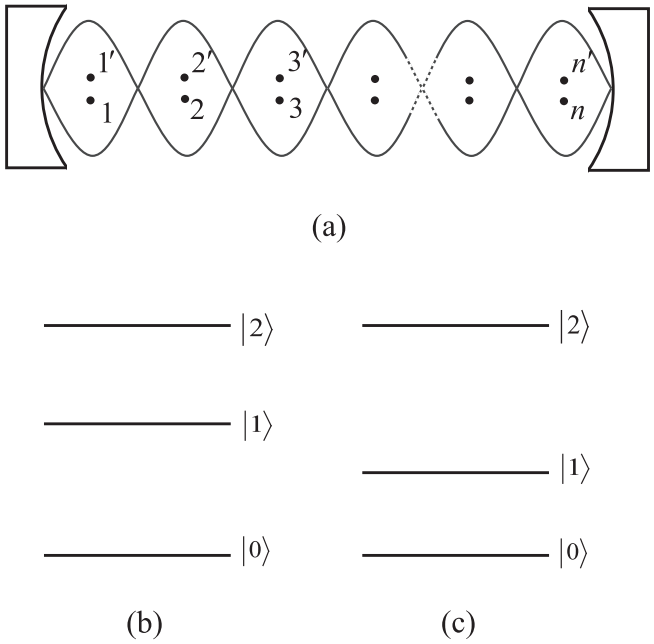

FIG. 2. (a) Diagram of qutrit pairs $\{1, 1'\}, \{2, 2'\}, \ldots, \{n, n'\}$ placed in a cavity or a resonator. The two periodic sinelike curves represent the standing-wave cavity mode. Each dark dot represents a qutrit. The two qutrits in each pair are arranged to be close, such that they couple to the environment in the same way appropriately. (b) Diagram of the three levels $|0\rangle$, $|1\rangle$, and $|2\rangle$ of a qutrit. Each horizontal line represents an energy level of the qutrit. The level spacing between the upper two levels is smaller than that between the two lowest levels. (c) Diagram of three levels $|0\rangle$, $|1\rangle$, and $|2\rangle$ of a qutrit. The level spacing between the upper two levels is greater than that between the two lowest levels. As shown in the next section, the $|0\rangle \leftrightarrow |1\rangle$ and $|1\rangle \leftrightarrow |2\rangle$ transitions are needed, while the $|0\rangle \leftrightarrow |2\rangle$ transition is not required for the gate realization. The level structure depicted in (b) is available in natural atoms, quantum dots, superconducting phase, transmon, and Xmon qutrits, while the level structure in (c) is achievable in nitrogen-vacancy centers, superconducting charge qutrits, flux qutrits, etc.

B. Qutrit-cavity resonant interaction

Consider now the cavity to be resonant with the $|0\rangle \leftrightarrow |1\rangle$ transition of qutrit 1 [Fig. 3(b)]. The Hamiltonian in the interaction picture and after the RWA is given by

$$H_2 = g_r \hat{a}|1\rangle_1\langle 0| + \text{H.c.}, \tag{4}$$

where the subscript 1 represents qutrit 1, g_r is the coupling constant of the cavity with the $|g\rangle \leftrightarrow |e\rangle$ transition, and $\hat{a}$

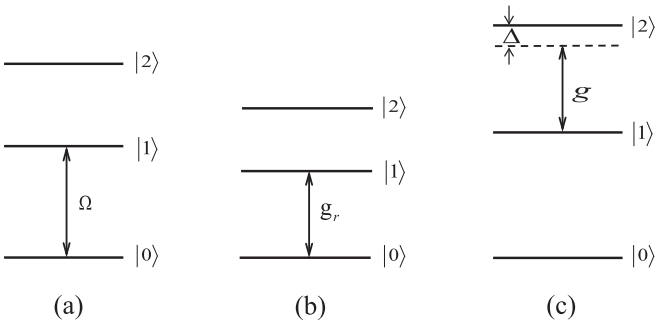

FIG. 3. (a) Illustration of a classical pulse resonant with the $|0\rangle \leftrightarrow |1\rangle$ transition of qutrit pairs $\{2, 2'\}, \{3, 3'\}, \ldots, \{n, n'\}$. Here, Ω is the pulse Rabi frequency. (b) Illustration of the cavity resonant with the $|0\rangle \leftrightarrow |1\rangle$ transition of qutrit 1, with coupling constant g_r. (c) Illustration of the cavity dispersively coupled to the $|1\rangle \leftrightarrow |2\rangle$ transition of qutrit pairs $\{2, 2'\}, \{3, 3'\}, \ldots, \{n, n'\}$ with coupling strength g and detuning $\Delta = \omega_{21} - \omega_c > 0$, while highly detuned (decoupled) from other energy-level transitions. The level spacings in (a), (b), and (c) are set to be different. Qutrits with the level spacings in (a) are decoupled from the cavity during the pulse. The level spacings of qutrits in (b) are adjusted such that the $|0\rangle \leftrightarrow |1\rangle$ transition is resonant with the cavity. The level spacings of qutrits in (c) are adjusted such that the $|1\rangle \leftrightarrow |2\rangle$ transition is dispersively coupled to the cavity. A double-arrow vertical line in (a) represents the pulse frequency, while a double-arrow vertical line in (b) and (c) represents the cavity frequency.

is the photon annihilation operator of the cavity. Under this Hamiltonian, we can obtain the state evolution

$$|1\rangle_1|0\rangle_c \rightarrow \cos g_r t|1\rangle_1|0\rangle_c - i \sin g_r t|0\rangle_1|1\rangle_c, \tag{5}$$

while the state $|0\rangle_1|0\rangle_c$ remains unchanged.

C. Qutrit-cavity dispersive interaction

Consider now the cavity to be dispersively coupled to the $|1\rangle \leftrightarrow |2\rangle$ transition of the qutrit pairs $\{2, 2'\}, \{3, 3'\}, \ldots, \{n, n'\}$, with coupling strength g and detuning $\Delta = \omega_{21} - \omega_c > 0$, while being highly detuned (decoupled) from other energy-level transitions [Fig. 3(c)]. Here, ω_{21} and ω_c are the $|1\rangle \leftrightarrow |2\rangle$ transition frequency of the qutrit pairs $\{2, 2'\}, \{3, 3'\}, \ldots, \{n, n'\}$ and the cavity frequency, respectively. The coupling or decoupling of qutrits with the cavity can be achieved by adjusting the qutrit's level spacings or the cavity frequency. For example, the level spacings of atoms or quantum dots can be adjusted by changing the voltage on the electrodes around each atom or quantum dot [52], the level spacings of NV centers can be readily changed by varying the external magnetic field applied along the crystalline axis of each NV center [53], and the level spacings of superconducting qutrits can be rapidly tuned within 1–3 ns [49,54]. In addition, the frequency of an optical cavity can be adjusted in experiments [55] and the frequency of a microwave cavity can be rapidly tuned with a few nanoseconds [56,57].

Under the above assumptions, the Hamiltonian of the system in the interaction picture and after the RWA is given by (assuming $\hbar = 1$)

$$H_3 = g e^{i\Delta t}\hat{a} \sum_{j=2}^{n} (|2\rangle_j\langle 1| + |2\rangle_{j'}\langle 1|) + \text{H.c.}, \tag{6}$$

where subscript j represents qutrit j ($j = 2, 3, \ldots, n$), while subscript j' represents qutrit j' ($j' = 2', 3', \ldots, n'$). For simplicity, in Eq. (6), we assume that the coupling strength g between the cavity and the $|1\rangle \leftrightarrow |2\rangle$ transition is the same for all of qutrit pairs $\{2, 2'\}, \{3, 3'\}, \ldots, \{n, n'\}$ for simplicity.

Under the large detuning condition $\Delta \gg g$, we can obtain the following effective Hamiltonian [58,59]:

$$\begin{aligned} H_{\text{eff}} = {} & \lambda \sum_{j=2}^{n} (|2\rangle_j\langle 2| + |2\rangle_{j'}\langle 2|)\hat{a}\hat{a}^+ \\ & - \lambda \sum_{j=2}^{n} (|1\rangle_j\langle 1| + |1\rangle_{j'}\langle 1|)\hat{a}^+\hat{a} \\ & + \lambda \sum_{j,k=2;j\neq k}^{n} |2\rangle_j\langle 1| \otimes |1\rangle_k\langle 2| \\ & + \lambda \sum_{j,k=2;j\neq k}^{n} |2\rangle_{j'}\langle 1| \otimes |1\rangle_{k'}\langle 2| \\ & + \lambda \sum_{j=2}^{n}\sum_{k'=2'}^{n'} |2\rangle_j\langle 1| \otimes |1\rangle_{k'}\langle 2| \\ & + \lambda \sum_{j=2}^{n}\sum_{k'=2'}^{n'} |1\rangle_j\langle 2| \otimes |2\rangle_{k'}\langle 1|, \end{aligned} \tag{7}$$

where $\lambda = g^2/\Delta$. Here, the terms in the first (second) bracket are ac-Stark shifts of the level $|2\rangle$ ($|1\rangle$) induced by the cavity. The last four terms represent the "dipole" coupling between qutrits, mediated by the cavity. When the level $|2\rangle$ of each qutrit is not occupied, the Hamiltonian (7) reduces to

$$H_{\text{eff}} = \sum_{j=2}^{n} H_{\text{eff},j}, \tag{8}$$

with

$$H_{\text{eff},j} = -\lambda(|1\rangle_j\langle 1| + |1\rangle_{j'}\langle 1|)\hat{a}^+\hat{a}, \tag{9}$$

where $H_{\text{eff},j}$ is the effective Hamiltonian of a subsystem, which consists of qutrit pair $\{j, j'\}$ and the cavity. Note that $[H_{\text{eff},j}, H_{\text{eff},k}] = 0$ ($j \neq k$). Thus the unitary operator $U = \exp(iH_{\text{eff}}t)$ can be expressed as $U = \prod_{j=2}^{n} \exp(iH_{\text{eff},j}t)$. Under the unitary operator U, one can easily find that the following state evolution

$$\begin{array}{l} |-_j +_{j'}\rangle|0\rangle_c \\ |+_j -_{j'}\rangle|0\rangle_c \\ |-_j +_{j'}\rangle|1\rangle_c \\ |+_j -_{j'}\rangle|1\rangle_c \end{array} \longrightarrow \begin{array}{c} |-_j +_{j'}\rangle|0\rangle_c \\ |+_j -_{j'}\rangle|0\rangle_c \\ \frac{(|0\rangle_j - e^{i\lambda t}|1\rangle_j)}{\sqrt{2}} \frac{(|0\rangle_{j'} + e^{i\lambda t}|1\rangle_{j'})}{\sqrt{2}}|1\rangle_c \\ \frac{(|0\rangle_j + e^{i\lambda t}|1\rangle_j)}{\sqrt{2}} \frac{(|0\rangle_{j'} - e^{i\lambda t}|1\rangle_{j'})}{\sqrt{2}}|1\rangle_c \end{array} \tag{10}$$

simultaneously applies to each of the qutrit pairs $\{2, 2'\}, \{3, 3'\}, \ldots, \{n, n'\}$. Here and below, $|\pm\rangle = (|0\rangle \pm |1\rangle)/\sqrt{2}$.

From the description given above, it can be seen that the state transformation (10) was obtained by assuming that the coupling strength g is the same for all the qutrit pairs $\{2, 2'\}, \{3, 3'\}, \ldots, \{n, n'\}$. However, this requirement is unnecessary. When the coupling strengths are nonidentical, it is straightforward to find that the Hamiltonian (9) can still be

achieved with λ now replaced by $\lambda = g_j^2/\Delta_j = g_{j'}^2/\Delta_{j'}$ ($j = 2, 3, \ldots, n$; $j' = 2', 3', \ldots, n'$). Here, g_j ($g_{j'}$) is the coupling strength between the cavity and the $|1\rangle \leftrightarrow |2\rangle$ transition of the qutrit j (j') and $\Delta_j = \omega_{21,j} - \omega_c$ ($\Delta_{j'} = \omega_{21,j'} - \omega_c$) is the detuning between the cavity frequency and the $|1\rangle \leftrightarrow |2\rangle$ transition frequency $\omega_{21,j}$ of the qutrit j (j'). Note that the condition $g_j^2/\Delta_j = g_{j'}^2/\Delta_{j'}$, i.e., $g_2^2/\Delta_2 = g_3^2/\Delta_3 = \cdots = g_n^2/\Delta_n = g_{2'}^2/\Delta_{2'} = g_{3'}^2/\Delta_{3'} = \cdots = g_{n'}^2/\Delta_{n'}$, can be met by carefully selecting the detunings via adjusting the level spacings of the qutrits.

In the next section, we will show how to use the above results (3), (5), and (10) to construct the gate described by Eq. (1).

IV. IMPLEMENTATION OF A MULTI-TARGET-QUBIT CONTROLLED-NOT GATE WITH LOGIC QUBITS OUTSIDE A DFS

For our gate implementation, the two logic states $|0\rangle$ and $|1\rangle$ of a physical qubit are represented by the two lowest levels $|0\rangle$ and $|1\rangle$ of a qutrit. In addition, the two logic states $|0_{L_j}\rangle$ and $|1_{L_j}\rangle$ of logic qubit j involved in Eq. (1) ($j = 1, 2, \ldots, n$) are encoded as $|0_{L_j}\rangle = |0_j 1_{j'}\rangle$ and $|1_{L_j}\rangle = |1_j 0_{j'}\rangle$ with two physical qubits $\{j, j'\}$ ($j, j' \in \{1, 1'\}, \{2, 2'\}, \ldots, \{n, n'\}$). Here, the two physical qubits $\{j, j'\}$ are associated with qutrit pair $\{j, j'\}$.

The procedure for implementing the multi-target-qubit controlled-NOT gate (1) is listed below.

Step (i). Apply a classical pulse (with $\phi = \pi/2$) to qutrit pairs $\{2, 2'\}, \ldots, \{n, n'\}$. The pulse is resonant with the $|0\rangle \leftrightarrow |1\rangle$ transition of the qutrits [Fig. 3(a)]. According to Eq. (3), after a pulse duration $\tau_1 = \pi/(2\Omega)$, we have the state transformation $|0\rangle \to |-\rangle$ and $|1\rangle \to |+\rangle$ for each of the qutrits $(2, 3, \ldots, n, 2', 3', \ldots, n')$.

Step (ii). Adjust the level spacing of qutrit 1 such that the $|0\rangle \leftrightarrow |1\rangle$ transition of qutrit 1 is resonant with the cavity [Fig. 3(b)]. According to Eq. (5), after an interaction time $\tau_2 = \pi/(2g_r)$, we have the state transformation $|1\rangle_1|0\rangle_c \to -i|0\rangle_1|1\rangle_c$, while the state $|0\rangle_1|0\rangle_c$ remains unchanged. After this step of operation, one should adjust the level spacing of qutrit 1 such that qutrit 1 is decoupled from the cavity.

Step (iii). Keep qutrit pair $\{1, 1'\}$ decoupled from the cavity but adjust the level spacing of qutrit pairs $\{2, 2'\}, \ldots, \{n, n'\}$ to obtain the effective Hamiltonian described by Eq. (8) [Fig. 3(c)]. According to Eq. (10), after an interaction time $\tau_3 = \pi/\lambda$, the following state transformation

$$\begin{array}{ll} |-_j +_{j'}\rangle|0\rangle_c & |-_j +_{j'}\rangle|0\rangle_c \\ |+_j -_{j'}\rangle|0\rangle_c & |+_j -_{j'}\rangle|0\rangle_c \\ |-_j +_{j'}\rangle|1\rangle_c & |+_j -_{j'}\rangle|1\rangle_c \\ |+_j -_{j'}\rangle|1\rangle_c & |-_j +_{j'}\rangle|1\rangle_c \end{array} \tag{11}$$

(where $j, j' \in \{1, 1'\}, \{2, 2'\}, \ldots, \{n, n'\}$) applies to each of the qutrit pairs $\{2, 2'\}, \{3, 3'\}, \ldots, \{n, n'\}$ simultaneously; i.e., the state of each qutrit remains unchanged when the cavity is in the vacuum state $|0\rangle_c$, while the state $|+\rangle$ of each qutrit flips to $|-\rangle$ or versus when the cavity is in the single photon state $|1\rangle_c$. After this step of the operation, one should adjust the level spacing of the qutrit pairs $\{2, 2'\}, \ldots, \{n, n'\}$, such that the qutrit pairs $\{2, 2'\}, \ldots, \{n, n'\}$ are decoupled from the cavity.

Step (iv). Adjust the level spacing of qutrit 1 such that the $|0\rangle \leftrightarrow |1\rangle$ transition of qutrit 1 is resonant with the cavity [Fig. 3(b)]. Let qutrit 1 interact with the cavity for a duration time $\tau_4 = 3\pi/(2g_r)$. As a result, we have $|0\rangle_1|1\rangle_c \to i|1\rangle_1|0\rangle_c$ according to Eq. (5). After this step of the operation, one should adjust the level spacing of qutrit 1 such that qutrit 1 is decoupled from the cavity.

Step (v). Apply a classical π pulse (with $\phi = -\pi/2$) to qutrit pairs $\{2, 2'\}, \ldots, \{n, n'\}$. The pulse is resonant with the $|0\rangle \leftrightarrow |1\rangle$ transition of qutrits for a duration time $\tau_5 = \pi/(4\Omega)$ [Fig. 3(a)], resulting in $|+\rangle \to |1\rangle$ and $|-\rangle \to |0\rangle$ for each qutrit according to Eq. (3).

One can check that the multi-target-qubit controlled-NOT gate of one logical qubit 1 simultaneously controlling $(n-1)$ target logical qubits $2, 3, \ldots, n$, described by Eq. (1), was realized with n qutrit pairs (i.e., the control qutrit pair $\{1, 1'\}$ and the target qutrit pairs $\{2, 2'\}, \ldots, \{n, n'\}$) after the above manipulation.

To understand more how the multiqubit phase gate described by Eq. (1) is realized by the above operations, let us now consider a three-logical-qubit example. One can check that the states of the whole system after each step of the above operations are summarized below:

$$\begin{array}{ll} |0_1 1_{1'}\rangle|0_2 1_{2'}\rangle|0_3 1_{3'}\rangle|0\rangle_c & |0_1 1_{1'}\rangle|-_2 +_{2'}\rangle|-_3 +_{3'}\rangle|0\rangle_c \\ |0_1 1_{1'}\rangle|0_2 1_{2'}\rangle|1_3 0_{3'}\rangle|0\rangle_c & |0_1 1_{1'}\rangle|-_2 +_{2'}\rangle|+_3 -_{3'}\rangle|0\rangle_c \\ |0_1 1_{1'}\rangle|1_2 0_{2'}\rangle|0_3 1_{3'}\rangle|0\rangle_c & |0_1 1_{1'}\rangle|+_2 -_{2'}\rangle|-_3 +_{3'}\rangle|0\rangle_c \\ |0_1 1_{1'}\rangle|1_2 0_{2'}\rangle|1_3 0_{3'}\rangle|0\rangle_c \xrightarrow{\text{Step (i)}} & |0_1 1_{1'}\rangle|+_2 -_{2'}\rangle|+_3 -_{3'}\rangle|0\rangle_c \xrightarrow{\text{Step (ii)}} \\ |1_1 0_{1'}\rangle|0_2 1_{2'}\rangle|0_3 1_{3'}\rangle|0\rangle_c & |1_1 0_{1'}\rangle|-_2 +_{2'}\rangle|-_3 +_{3'}\rangle|0\rangle_c \\ |1_1 0_{1'}\rangle|0_2 1_{2'}\rangle|1_3 0_{3'}\rangle|0\rangle_c & |1_1 0_{1'}\rangle|-_2 +_{2'}\rangle|+_3 -_{3'}\rangle|0\rangle_c \\ |1_1 0_{1'}\rangle|1_2 0_{2'}\rangle|0_3 1_{3'}\rangle|0\rangle_c & |1_1 0_{1'}\rangle|+_2 -_{2'}\rangle|-_3 +_{3'}\rangle|0\rangle_c \\ |1_1 0_{1'}\rangle|1_2 0_{2'}\rangle|1_3 0_{3'}\rangle|0\rangle_c & |1_1 0_{1'}\rangle|+_2 -_{2'}\rangle|+_3 -_{3'}\rangle|0\rangle_c \end{array}$$

$$\begin{array}{ll} |0_1 1_{1'}\rangle|-_2 +_{2'}\rangle|-_3 +_{3'}\rangle|0\rangle_c & |0_1 1_{1'}\rangle|-_2 +_{2'}\rangle|-_3 +_{3'}\rangle|0\rangle_c \\ |0_1 1_{1'}\rangle|-_2 +_{2'}\rangle|+_3 -_{3'}\rangle|0\rangle_c & |0_1 1_{1'}\rangle|-_2 +_{2'}\rangle|+_3 -_{3'}\rangle|0\rangle_c \\ |0_1 1_{1'}\rangle|+_2 -_{2'}\rangle|-_3 +_{3'}\rangle|0\rangle_c & |0_1 1_{1'}\rangle|+_2 -_{2'}\rangle|-_3 +_{3'}\rangle|0\rangle_c \\ |0_1 1_{1'}\rangle|+_2 -_{2'}\rangle|+_3 -_{3'}\rangle|0\rangle_c \xrightarrow{\text{Step (iii)}} & |0_1 1_{1'}\rangle|+_2 -_{2'}\rangle|+_3 -_{3'}\rangle|0\rangle_c \\ -i|0_1 0_{1'}\rangle|-_2 +_{2'}\rangle|-_3 +_{3'}\rangle|1\rangle_c & -i|0_1 0_{1'}\rangle|+_2 -_{2'}\rangle|+_3 -_{3'}\rangle|1\rangle_c \\ -i|0_1 0_{1'}\rangle|-_2 +_{2'}\rangle|+_3 -_{3'}\rangle|1\rangle_c & -i|0_1 0_{1'}\rangle|+_2 -_{2'}\rangle|-_3 +_{3'}\rangle|1\rangle_c \\ -i|0_1 0_{1'}\rangle|+_2 -_{2'}\rangle|-_3 +_{3'}\rangle|1\rangle_c & -i|0_1 0_{1'}\rangle|-_2 +_{2'}\rangle|+_3 -_{3'}\rangle|1\rangle_c \\ -i|0_1 0_{1'}\rangle|+_2 -_{2'}\rangle|+_3 -_{3'}\rangle|1\rangle_c & -i|0_1 0_{1'}\rangle|-_2 +_{2'}\rangle|-_3 +_{3'}\rangle|1\rangle_c \end{array}$$

$$\begin{array}{l} |0_1 1_{1'}\rangle|-_2 +_{2'}\rangle|-_3 +_{3'}\rangle|0\rangle_c \\ |0_1 1_{1'}\rangle|-_2 +_{2'}\rangle|+_3 -_{3'}\rangle|0\rangle_c \\ |0_1 1_{1'}\rangle|+_2 -_{2'}\rangle|-_3 +_{3'}\rangle|0\rangle_c \\ \xrightarrow{\text{Step (iv)}} |0_1 1_{1'}\rangle|+_2 -_{2'}\rangle|+_3 -_{3'}\rangle|0\rangle_c \\ |1_1 0_{1'}\rangle|+_2 -_{2'}\rangle|+_3 -_{3'}\rangle|0\rangle_c \\ |1_1 0_{1'}\rangle|+_2 -_{2'}\rangle|-_3 +_{3'}\rangle|0\rangle_c \\ |1_1 0_{1'}\rangle|-_2 +_{2'}\rangle|+_3 -_{3'}\rangle|0\rangle_c \\ |1_1 0_{1'}\rangle|-_2 +_{2'}\rangle|-_3 +_{3'}\rangle|0\rangle_c \end{array} \begin{array}{l} \\ \\ \\ \xrightarrow{\text{Step (v)}} \\ \\ \\ \\ \\ \end{array} \begin{array}{l} |0_1 1_{1'}\rangle|0_2 1_{2'}\rangle|0_3 1_{3'}\rangle|0\rangle_c \\ |0_1 1_{1'}\rangle|0_2 1_{2'}\rangle|1_3 0_{3'}\rangle|0\rangle_c \\ |0_1 1_{1'}\rangle|1_2 0_{2'}\rangle|0_3 1_{3'}\rangle|0\rangle_c \\ |0_1 1_{1'}\rangle|1_2 0_{2'}\rangle|1_3 0_{3'}\rangle|0\rangle_c \\ |1_1 0_{1'}\rangle|1_2 0_{2'}\rangle|1_3 0_{3'}\rangle|0\rangle_c, \\ |1_1 0_{1'}\rangle|1_2 0_{2'}\rangle|0_3 1_{3'}\rangle|0\rangle_c \\ |1_1 0_{1'}\rangle|0_2 1_{2'}\rangle|1_3 0_{3'}\rangle|0\rangle_c \\ |1_1 0_{1'}\rangle|0_2 1_{2'}\rangle|0_3 1_{3'}\rangle|0\rangle_c \end{array} \tag{12}$$

which shows that a three-logical-qubit controlled-NOT gate, described by

$$\begin{aligned} &|0_1 1_{1'}\rangle|0_j 1_{j'}\rangle|0_j 1_{j'}\rangle \to |0_1 1_{1'}\rangle|0_j 1_{j'}\rangle|0_j 1_{j'}\rangle, \\ &|0_1 1_{1'}\rangle|0_j 1_{j'}\rangle|1_j 0_{j'}\rangle \to |0_1 1_{1'}\rangle|0_j 1_{j'}\rangle|1_j 0_{j'}\rangle, \\ &|0_1 1_{1'}\rangle|1_j g_{j'}\rangle|0_j 1_{j'}\rangle \to |0_1 1_{1'}\rangle|1_j 0_{j'}\rangle|0_j 1_{j'}\rangle, \\ &|0_1 1_{1'}\rangle|1_j 0_{j'}\rangle|1_j 0_{j'}\rangle \to |0_1 1_{1'}\rangle|1_j 0_{j'}\rangle|1_j 0_{j'}\rangle, \\ &|1_1 0_{1'}\rangle|0_j 1_{j'}\rangle|0_j 1_{j'}\rangle \to |1_1 0_{1'}\rangle|1_j 0_{j'}\rangle|1_j 0_{j'}\rangle, \\ &|1_1 0_{1'}\rangle|0_j 1_{j'}\rangle|1_j 0_{j'}\rangle \to |1_1 0_{1'}\rangle|1_j 0_{j'}\rangle|0_j 1_{j'}\rangle, \\ &|1_1 0_{1'}\rangle|1_j 0_{j'}\rangle|0_j 1_{j'}\rangle \to |1_1 0_{1'}\rangle|0_j 1_{j'}\rangle|1_j 0_{j'}\rangle, \\ &|1_1 0_{1'}\rangle|1_j 0_{j'}\rangle|1_j 0_{j'}\rangle \to |1_1 0_{1'}\rangle|0_j 1_{j'}\rangle|0_j 1_{j'}\rangle \end{aligned} \tag{13}$$

or

$$\begin{aligned} &|0_{L_1}\rangle|0_{L_2}\rangle|0_{L_3}\rangle \to |0_{L_1}\rangle|0_{L_2}\rangle|0_{L_3}\rangle, \\ &|0_{L_1}\rangle|0_{L_2}\rangle|1_{L_3}\rangle \to |0_{L_1}\rangle|0_{L_2}\rangle|1_{L_3}\rangle, \\ &|0_{L_1}\rangle|1_{L_2}\rangle|1_{L_3}\rangle \to |0_{L_1}\rangle|1_{L_2}\rangle|0_{L_3}\rangle, \\ &|0_{L_1}\rangle|1_{L_2}\rangle|1_{L_3}\rangle \to |0_{L_1}\rangle|1_{L_2}\rangle|1_{L_3}\rangle, \\ &|1_{L_1}\rangle|0_{L_2}\rangle|0_{L_3}\rangle \to |1_{L_1}\rangle|1_{L_2}\rangle|1_{L_3}\rangle, \\ &|1_{L_1}\rangle|0_{L_2}\rangle|1_{L_3}\rangle \to |1_{L_1}\rangle|1_{L_2}\rangle|0_{L_3}\rangle, \\ &|1_{L_1}\rangle|1_{L_2}\rangle|0_{L_3}\rangle \to |1_{L_1}\rangle|0_{L_2}\rangle|1_{L_3}\rangle, \\ &|1_{L_1}\rangle|1_{L_2}\rangle|1_{L_3}\rangle \to |1_{L_1}\rangle|0_{L_2}\rangle|0_{L_3}\rangle \end{aligned} \tag{14}$$

(with the control logical qubit 1 simultaneously controlling two target logical qubits 2 and 3) was achieved with three qutrit pairs $\{1, 1'\}$, $\{2, 2'\}$, $\{3, 3'\}$ (i.e., the control qutrit pair $\{1, 1'\}$ and the two target qutrit pairs $\{2, 2'\}$ and $\{3, 3'\}$) after the previous process.

From the description given above, the following can be seen.

(i) During the gate operation, the states of the logical qubits are manipulated outside the DFS. However, the states of the logical qubits return to the DFS after the gate operation.

(ii) The same detuning Δ is set for qutrit pairs $\{2, 2'\}, \{3, 3'\}, \ldots, \{n, n'\}$. Therefore, the level spacings of qutrit pairs $\{2, 2'\}, \{3, 3'\}, \ldots, \{n, n'\}$ can be synchronously tuned through changing the common external parameters.

(iii) The level $|2\rangle$ for all qutrits is not occupied during the entire operation. Hence decoherence caused by energy relaxation and dephasing of this intermediate higher-energy level is greatly suppressed.

(iv) This proposal does not require measurement on the state of the qutrits or the cavity. Thus the gate is implemented deterministically.

(v) The total operation time is

$$t_{\text{op}} = \pi/\lambda + 2\pi/g_r + \pi/\Omega + 6\tau_d, \tag{15}$$

which is independent of the number of logic qubits and thus does not increase with the number of logic qubits. Here, τ_d is the typical time required for adjusting the level spacings of the qutrits.

It is necessary to give a brief discussion on experimental matters. Several points are made as follows.

(i) To make the effect of decoherence from the qutrits negligible, the total operation time t_{op} should be much smaller than the energy relaxation time T_1 and the dephasing time T_2 of the level $|1\rangle$ as well as the energy relaxation time T_1' and the dephasing time T_2' of the level $|2\rangle$. Note that $t_{\text{op}} \ll T_1', T_2'$ can be readily met because the level $|2\rangle$ is unpopulated during the entire operation. In addition, $t_{\text{op}} \ll T_1, T_2$ can be achieved by choosing qutrits with sufficiently long energy relaxation time T_1 and dephasing time T_2 of the level $|1\rangle$. Alternatively, these conditions can be met by shortening t_{op}. Note that t_{op} can be shortened by increasing g_r, Ω (via increasing the pulse intensity), and λ (through an optimal choice of the ratio Δ/g).

(ii) To have the cavity dissipation negligibly small, the total operation time t_{op} should be much shorter than the photon lifetime κ^{-1} of the cavity, which is given by $\kappa^{-1} = Q/\omega_c$. Here, Q is the (loaded) quality factor of the cavity. Note that the condition $t_{\text{op}} \ll \kappa^{-1}$ can be achieved by employing a high-Q cavity or shortening t_{op}.

Before ending this section, we should mention that for steps (ii) and (iv) above, adjusting the level spacings of the qutrit 1 could induce a phase shift $e^{i\phi}$ on the state $|1\rangle$ of the qutrit 1 and, for step (ii) above, adjusting the level spacings of the qutrit pairs $\{2, 2'\}, \{3, 3'\}, \ldots, \{n, n'\}$ causes a phase shift $e^{i\varphi}$ on the state $|1\rangle$ of each of the qutrits $\{2, 2', 3, 3', \ldots, n, n'\}$. Note that the effect of the unwanted phase shifts here can be eliminated by a proper control of the level adjustment (e.g., the adjusting speed or/and the amount of the energy to be adjusted) such that $\phi = 2m\pi$ and $\varphi = 2k\pi$ (m and k are integers).

V. APPLICATION: CREATING GHZ STATES OF MULTIPLE LOGIC QUBITS IN A DFS

GHZ entangled states have many applications in quantum information processing. To date, GHZ states of 10 or more *physical qubits* have been experimentally demonstrated in various systems [60–65]. Theoretically, a large number of theoretical methods have been presented for creating GHZ states of multiple *physical qubits* with different kinds of

quantum systems [66–80]. However, how to prepare GHZ states with *logical qubits* encoded in DFS has rarely been investigated. In the following, we will show how to apply the proposed gate to create GHZ states of multiple logical qubits encoded in a DFS.

Consider n qutrit pairs $\{1, 1'\}, \{2, 2'\}, \ldots, \{n, n'\}$ placed in a single cavity or coupled to a resonator. The n qutrit pairs are initially decoupled from the cavity. The qutrit pair $\{1, 1'\}$ is initially in the state $|1_1 0_{1'}\rangle$, while each of the qutrit pairs $\{2, 2'\}, \{3, 3'\}, \ldots, \{n, n'\}$ is initially in the state $|0_j 1_{j'}\rangle$ ($j, j' \in \{1, 1'\}, \{2, 2'\}, \ldots, \{n, n'\}$). The cavity is initially in the vacuum state $|0\rangle_c$. The procedure for creating GHZ states of n logic qubits is given as follows.

Step (i). Adjust the level spacing of qutrit 1 such that the $|0\rangle \leftrightarrow |1\rangle$ transition of qutrit 1 is resonant with the cavity [Fig. 3(b)]. Let qutrit 1 interact with the cavity for an interaction time $\tau_1' = \pi/(2g_r)$. According to Eq. (5), we have $|1_1 0_{1'}\rangle|0\rangle_c \to -i|0_1 0_{1'}\rangle|1\rangle_c$. After this operation, one should adjust the level spacing of qutrit 1 such that qutrit 1 is decoupled from the cavity.

Step (ii). Adjust the level spacing of the qutrit pair $\{1, 1'\}$ such that the $|0\rangle \leftrightarrow |1\rangle$ transition of the qutrit pair $\{1, 1'\}$ is resonant with the cavity [Fig. 3(b)]. The Hamiltonian in the interaction picture becomes

$$H_4 = g_r \hat{a}(|1\rangle_1\langle 0| + |1\rangle_{1'}\langle 0|) + \text{H.c.}, \tag{16}$$

where subscript 1 represents qutrit 1 and subscript $1'$ represents qutrit $1'$. Under this Hamiltonian, one can obtain the state evolution $|0_1 0_{1'}\rangle|1\rangle_c \to \cos(\sqrt{2}g_r t)|0_1 0_{1'}\rangle|1\rangle_c - i\sin(\sqrt{2}g_r t)(|0_1 1_{1'}\rangle + |1_1 0_{1'}\rangle)|0\rangle_c/\sqrt{2}$. Let now qutrit pair $\{1, 1'\}$ interact with the cavity for an interaction time $\tau_2' = \pi/(2\sqrt{2}g_r)$. As a result, we have the state transformation $|0_1 0_{1'}\rangle|1\rangle_c \to -i(|0_1 1_{1'}\rangle + |1_1 0_{1'}\rangle)|0\rangle_c/\sqrt{2}$. After this operation, one should adjust the level spacing of qutrit pair $\{1, 1'\}$ such that qutrit pair $\{1, 1'\}$ is decoupled from the cavity.

Steps (iii)–(vii). The operations of steps (iii)–(vii) here are the operations of steps (i)–(v) described in the previous section, which implements the multi-target-qubit controlled-NOT gate (1). By applying this gate, one can achieve the following state transformation:

$$\begin{aligned}
&|0_1 1_{1'}\rangle|0_2 1_{2'}\rangle|0_3 1_{3'}\rangle \ldots |0_n 1_{n'}\rangle|0\rangle_c \to |0_1 1_{1'}\rangle|0_2 1_{2'}\rangle|0_3 1_{3'}\rangle \ldots |0_n 1_{n'}\rangle|0\rangle_c,\\
&|1_1 0_{1'}\rangle|0_2 1_{2'}\rangle|0_3 1_{3'}\rangle \ldots |0_n 1_{n'}\rangle|0\rangle_c \to |1_1 0_{1'}\rangle|1_2 0_{2'}\rangle|1_3 0_{3'}\rangle \ldots |1_n 0_{n'}\rangle|0\rangle_c.
\end{aligned} \tag{17}$$

One can check that the states of the whole system after the above operations are summarized below:

$$\begin{aligned}
&|1_1 0_{1'}\rangle|0_2 1_{2'}\rangle|0_3 1_{3'}\rangle \ldots |0_n 1_{n'}\rangle|0\rangle_c \xrightarrow{\text{Step (i)}} -i|0_1 0_{1'}\rangle|0_2 1_{2'}\rangle|0_3 1_{3'}\rangle \ldots |0_n 1_{n'}\rangle|1\rangle_c\\
&\xrightarrow{\text{Step (ii)}} -\frac{1}{\sqrt{2}}(|0_1 1_{1'}\rangle + |1_1 0_{1'}\rangle)|0_2 1_{2'}\rangle|0_3 1_{3'}\rangle \ldots |0_n 1_{n'}\rangle|0\rangle_c \xrightarrow{\text{Steps (iii)–(vii)}}\\
&-\frac{1}{\sqrt{2}}(|0_1 1_{1'}\rangle|0_2 1_{2'}\rangle|0_3 1_{3'}\rangle \ldots |0_n 1_{n'}\rangle + |1_1 0_{1'}\rangle|1_2 0_{2'}\rangle|1_3 0_{3'}\rangle \ldots |1_n 0_{n'}\rangle)|0\rangle_c.
\end{aligned} \tag{18}$$

The last line of Eq. (18) can be rewritten as

$$\frac{1}{\sqrt{2}}\left(|0_{L_1}\rangle|0_{L_2}\rangle \ldots |0_{L_n}\rangle + |1_{L_1}\rangle|1_{L_2}\rangle \ldots |1_{L_n}\rangle\right)|0\rangle_c, \tag{19}$$

which shows that the cavity returns to its initial vacuum state while the n qutrit pairs $\{1, 1'\}, \{2, 2'\}, \ldots, \{n, n'\}$ are prepared in a GHZ state $\frac{1}{\sqrt{2}}(|0_{L_1}\rangle|0_{L_2}\rangle \ldots |0_{L_n}\rangle + |1_{L_1}\rangle|1_{L_2}\rangle \ldots |1_{L_n}\rangle)$ of n logical qubits encoded in the DFS.

The total operation time for the GHZ state preparation is

$$t_{\text{op}}' = \pi/\lambda + (5\sqrt{2}+1)\pi/(2\sqrt{2}g_r) + \pi/\Omega + 10\tau_d, \tag{20}$$

which should be much smaller than the energy relaxation time T_1 and the dephasing time T_2 of the level $|1\rangle$, the energy relaxation time T_1' and the dephasing time T_2' of the level $|2\rangle$, and the photon lifetime κ^{-1} of the cavity.

VI. EXPERIMENTAL FEASIBILITY FOR CREATING GHZ STATES OF THREE LOGIC QUBITS IN A DFS

Above we have considered a generic kind of physical qubit, whose two logical states are represented by the two lowest levels of a qutrit. Circuit QED, consisting of microwave cavities and superconducting (SC) qubits, is an analog of cavity QED and has been considered as one of the leading candidates for quantum information processing (for reviews, see [81–87]). In this section, we investigate the experimental feasibility for creating the GHZ state of three logical qubits in a DFS by using three pairs of superconducting (SC) transmon qutrits $\{1, 1'\}$, $\{2, 2'\}$, and $\{3, 3'\}$, which are coupled to a one-dimensional coplanar waveguide resonator (Fig. 4). Compared to a Cooper pair box, a transmon has a longer decoherence time, which is constructed by shunting a large capacitance on the two Josephson junctions of a Cooper pair box [88]. The idea of shunting a large capacitance on the

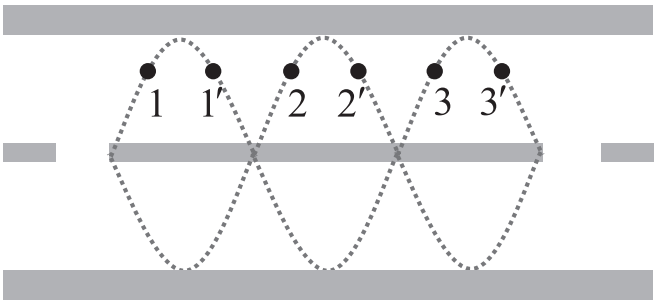

FIG. 4. Setup for six superconducting transmon qutrits (dark dots) embedded in a one-dimensional coplanar waveguide resonator. The two periodic sinelike curved lines represent the standing-wave magnetic field of the resonator.

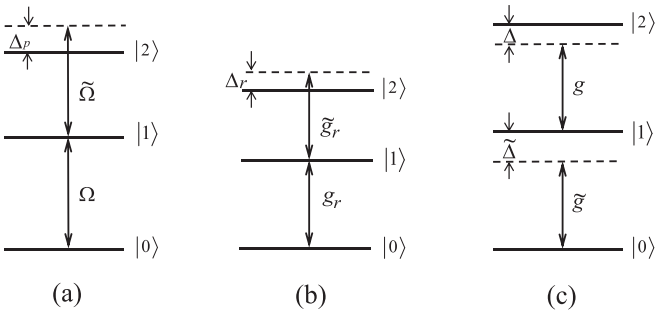

FIG. 5. (a) Classical pulse is resonant with the $|0\rangle \leftrightarrow |1\rangle$ transition of the qutrit pairs $\{2, 2'\}, \{3, 3'\}$ with a Rabi frequency Ω, while being off resonant with the $|1\rangle \leftrightarrow |2\rangle$ transition of qutrit pairs $\{2, 2'\}, \{3, 3'\}$ with Rabi frequency $\widetilde{\Omega}$ and detuning Δ_p. (b) The cavity is resonant with the $|0\rangle \leftrightarrow |1\rangle$ transition of qutrit 1 ($1'$) with coupling constant g_r, while off resonant with the $|1\rangle \leftrightarrow |2\rangle$ transition of qutrit 1 ($1'$) with coupling constant $\widetilde{g}_r$ and detuning Δ_r. (c) The cavity is dispersively coupled to the $|1\rangle \leftrightarrow |2\rangle$ transition of qutrit pairs $\{2, 2'\}, \{3, 3'\}$ with coupling strength g and detuning $\Delta = \omega_{21} - \omega_c > 0$, while off resonant with the $|0\rangle \leftrightarrow |1\rangle$ transition of qutrit pairs $\{2, 2'\}, \{3, 3'\}$ with coupling strength $\widetilde{g}$ and detuning $\widetilde{\Delta} = \omega_{10} - \omega_c > 0$.

Josephson junctions to increase decoherence was also earlier proposed for a superconducting flux qubit [89].

Based on the above discussion, it can be seen that four basic qutrit-cavity or qutrit-pulse interactions are used in the GHZ-state preparation, i.e., the three basic interactions described by the Hamiltonians H_1, H_2, H_3 for the gate realization, plus the basic interaction described by the Hamiltonian H_4. After considering the unwanted interactions, the Hamiltonians are modified as follows.

(i) $H_1' = H_1 + \delta H_1$, where δH_1 describes the unwanted interaction between the pulse and the $|1\rangle \leftrightarrow |2\rangle$ transition of the qutrit pairs $\{2, 2'\}, \{3, 3'\}$ [Fig. 5(a)]. The expression of δH_1 is given by

$$\delta H_1 = \widetilde{\Omega}\, e^{-i\phi} e^{i\Delta_p t} \sum_{j=2}^{3} (|2\rangle_j\langle 1| + |2\rangle_{j'}\langle 1|) + \text{H.c.}, \tag{21}$$

where $\widetilde{\Omega}$ is the pulse Rabi frequency associated with the $|1\rangle \leftrightarrow |2\rangle$ transition of the qutrit pairs $\{2, 2'\}, \{3, 3'\}$, and $\Delta_p = \omega_{21} - \omega_p = \omega_{21} - \omega_{10} < 0$ is the detuning between the pulse frequency and the $|1\rangle \leftrightarrow |2\rangle$ transition frequency of the qutrit pairs $\{2, 2'\}, \{3, 3'\}$.

(ii) $H_2' = H_2 + \delta H_2$, where δH_2 describes the unwanted interaction between the cavity and the $|1\rangle \leftrightarrow |2\rangle$ transition of the qutrit 1 [Fig. 5(b)]. The expression of δH_2 is given by

$$\delta H_2 = \widetilde{g}_r e^{i\Delta_r t} a |2\rangle_1\langle 1| + \text{H.c.}, \tag{22}$$

where $\widetilde{g}_r$ is the coupling strength between the cavity and the $|1\rangle \leftrightarrow |2\rangle$ transition of the qutrit 1 and $\Delta_r = \omega_{21} - \omega_c < 0$ is the detuning between the cavity frequency and the $|1\rangle \leftrightarrow |2\rangle$ transition frequency of the qutrit 1.

(iii) $H_3' = H_3 + \delta H_3$, where δH_3 describes the unwanted interaction between the cavity and the $|0\rangle \leftrightarrow |1\rangle$ transition of the qutrit pairs $\{2, 2'\}, \{3, 3'\}$ [Fig. 5(c)]. Here, H_3 is the Hamiltonian given in Eq. (6), with $n = 3$. The expression of δH_3 is given by

$$\delta H_3 = \widetilde{g}\, e^{i\widetilde{\Delta}t} \hat{a} \sum_{j=2}^{3} (|1\rangle_j\langle 0| + |1\rangle_{j'}\langle 0|) + \text{H.c.}, \tag{23}$$

where $\widetilde{g}$ is the coupling strength between the cavity and the $|0\rangle \leftrightarrow |1\rangle$ transition of the qutrit pairs $\{2, 2'\}, \{3, 3'\}$, and $\widetilde{\Delta} = \omega_{10} - \omega_c$ is the detuning between the cavity frequency and the $|0\rangle \leftrightarrow |1\rangle$ transition frequency of the qutrit pairs $\{2, 2'\}, \{3, 3'\}$.

(iv) $H_4' = H_4 + \delta H_4$, where δH_4 describes the unwanted interaction between the cavity and the $|1\rangle \leftrightarrow |2\rangle$ transition of the qutrit pair $\{1, 1'\}$ [Fig. 5(b)]. The expression of δH_4 is given by

$$\delta H_4 = \widetilde{g}_r e^{i\Delta_r t} \hat{a} (|2\rangle_1\langle 1| + |2\rangle_{1'}\langle 1|) + \text{H.c.} \tag{24}$$

It is noted that the $|0\rangle \leftrightarrow |2\rangle$ transition of qutrits induced by the pulse or the cavity is negligible because of $\omega_{10}, \omega_{21} \ll \omega_{20}$ (Fig. 5). In addition, during the adjustment of the qutrit level spacings, the effect of the qutrit decoherence and the cavity decay is negligible because the level spacings of transmon qutrits can be rapidly adjusted within 1–2 ns.

With the qutrit decoherence and the cavity dissipation taken into account, the dynamics of the whole system, under the Markovian approximation, is governed by the master equation

$$\begin{aligned}\frac{d\rho}{dt} = &-i[H_k', \rho] + \kappa\mathcal{L}[\hat{a}] + \gamma_{21}\sum_{j=1}^{3}\mathcal{L}[\sigma_{f21,j}^{-}] \\ &+ \gamma_{20}\sum_{j=1}^{3}\mathcal{L}[\sigma_{20,j}^{-}] + \gamma_{10}\sum_{j=1}^{3}\mathcal{L}[\sigma_{10,j}^{-}] + \gamma_{21}\sum_{j=1}^{3}\mathcal{L}[\sigma_{21,j'}^{-}] \\ &+ \gamma_{20}\sum_{j=1}^{3}\mathcal{L}[\sigma_{20,j'}^{-}] + \gamma_{10}\sum_{j=1}^{3}\mathcal{L}[\sigma_{10,j'}^{-}] \\ &+ \sum_{j=1}^{3}\sum_{l=1,2}\gamma_{\varphi,l}(\sigma_{ll,j}\rho\sigma_{ll,j} - \sigma_{ll,j}\rho/2 - \rho\sigma_{ll,j}/2) \\ &+ \sum_{j=1}^{3}\sum_{l=1,2}\gamma_{\varphi,l}(\sigma_{ll,j'}\rho\sigma_{ll,j'} - \sigma_{ll,j'}\rho/2 - \rho\sigma_{ll,j'}/2),\end{aligned} \tag{25}$$

where H_k' (with $k = 1, 2, 3, 4$) are the above-modified Hamiltonians H_1', H_2', H_3', and H_4', $\mathcal{L}[\Lambda] = \Lambda\rho\Lambda^{+} - \Lambda^{+}\Lambda\rho/2 - \rho\Lambda^{+}\Lambda/2$ (with $\Lambda = \hat{a}, , \sigma_{21,j}^{-}, \sigma_{20,j}^{-}, \sigma_{10,j}^{-}, \sigma_{21,j'}^{-}, \sigma_{20,j'}^{-}, \sigma_{10,j'}^{-}$), $\sigma_{21,j}^{-} = |1\rangle_j\langle 2|$, $\sigma_{20,j}^{-} = |0\rangle_j\langle 2|$, $\sigma_{10,j}^{-} = |0\rangle_j\langle 1|$, $\sigma_{21,j'}^{-} = |1\rangle_{j'}\langle 2|$, $\sigma_{20,j'}^{-} = |0\rangle_{j'}\langle 2|$, $\sigma_{10,j'}^{-} = |0\rangle_{j'}\langle 1|$, $\sigma_{11,j} = |1\rangle_j\langle 1|$, $\sigma_{22,j} = |2\rangle_j\langle 2|$, $\sigma_{11,j'} = |1\rangle_{j'}\langle 1|$, and $\sigma_{22,j'} = |2\rangle_{j'}\langle 2|$. In addition, κ is the decay rate of the cavity, γ_{10} is the energy relaxation rate for the level $|1\rangle$ of qutrits associated with the decay path $|1\rangle \to |0\rangle$, γ_{21} (γ_{20}) is the relaxation rate for the level $|2\rangle$ of qutrits related to the decay path $|2\rangle \to |1\rangle$ ($|2\rangle \to |0\rangle$), and $\gamma_{\varphi,1}$ ($\gamma_{\varphi,2}$) is the dephasing rate of the level $|1\rangle$ ($|2\rangle$) of qutrits.

The fidelity of the entire operation is given by $\mathcal{F} = \sqrt{\langle\psi_{id}|\rho|\psi_{id}\rangle}$, where $|\psi_{id}\rangle$ is the ideal output state given by $\frac{1}{\sqrt{2}}(|0_{L_1}\rangle|0_{L_2}\rangle|0_{L_3}\rangle + |1_{L_1}\rangle|1_{L_2}\rangle|1_{L_3}\rangle)|0\rangle_c$ [i.e., the state given

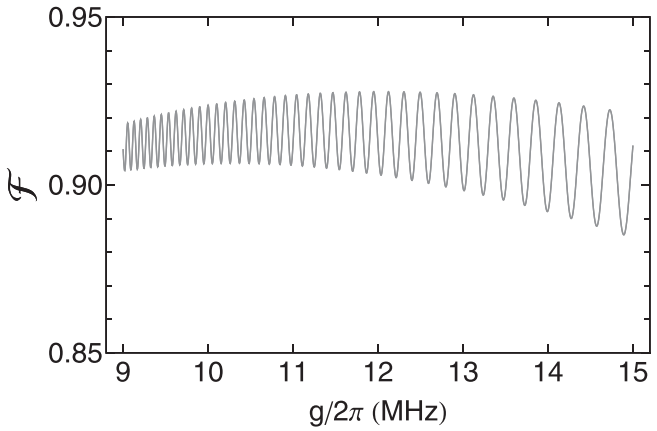

FIG. 6. Fidelity versus g. The figure is plotted for $\Omega/2\pi = 22$ MHz.

in Eq. (19) for $n = 3$], while ρ is the final density matrix obtained by numerically solving the master equation.

We now numerically calculate the fidelity. For a transmon qutrit, the level spacing anharmonicity $\delta/2\pi = (\omega_{10} - \omega_{21})/2\pi = 100$–$700$ MHz was reported in experiments [90]. As an example, consider $\delta/2\pi = 0.7$ GHz and $\Delta/2\pi = 0.1$ GHz. Thus we have $\widetilde{\Delta}/2\pi = 0.8$ GHz and $\Delta_r/2\pi = \Delta_p/2\pi = -0.7$ GHz. For simplicity, we assume $g = g_r$. For a transmon qutrit [88], $\widetilde{g} = g/\sqrt{2}$, $\widetilde{g}_r = \sqrt{2}g_r$, and $\widetilde{\Omega} = \sqrt{2}\Omega$. Other parameters used in the numerical simulation are (i) $\gamma_{10}^{-1} = 60$ μs, $\gamma_{20}^{-1} = 150$ μs [91], $\gamma_{21}^{-1} = 30$ μs, $\gamma_{\phi,1}^{-1} = \gamma_{\phi,2}^{-1} = 20$ μs, and (ii) $\kappa^{-1} = 10$ μs. Here, we consider a rather conservative case for decoherence time of the transmon qutrits [92,93].

By solving the master equation (25), we numerically calculate the fidelity. Figure 6 shows the fidelity versus g, while Fig. 7 shows the fidelity versus Ω. Figure 6 (7) demonstrates that the fidelity strongly depends on the value of g (Ω). From Fig. 6 or Fig. 7, it can be seen that, for $g/2\pi = 12.5$ MHz and $\Omega/2\pi = 22$ MHz, a high fidelity 92.8% can be achieved. For $g/2\pi = 12.5$ MHz, we have $g_r/2\pi = 12.5$ MHz, $\widetilde{g}/2\pi = 8.84$ MHz, and $\widetilde{g}_r/2\pi = 17.67$ MHz, which are readily available in experiments because a coupling strength $g/2\pi \sim 360$ MHz has been reported for a transmon qutrit coupled to a TLR [12,94].

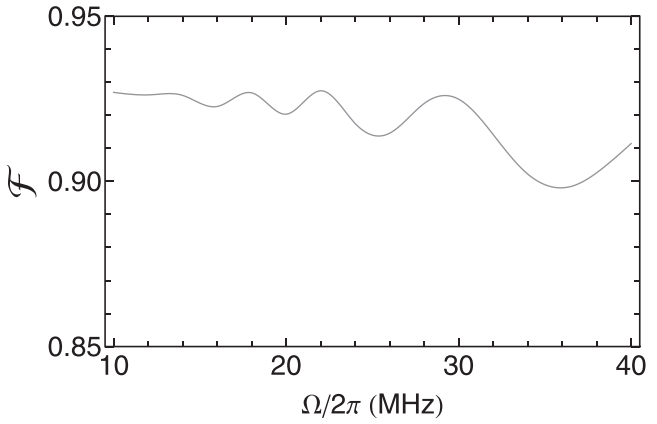

FIG. 7. Fidelity versus Ω. The figure is plotted for $g/2\pi = 12.5$ MHz.

Note that the influence of the third-excited state $|3\rangle$ of the transmon can be neglected. This is because (i) due to the use of the large detuning (see Fig. 5), the population of the state $|3\rangle$ of the transmon is very small and (ii) there exists a larger detuning between the cavity frequency (the pulse frequency) and the $|2\rangle \leftrightarrow |3\rangle$ transition frequency, compared to the detuning between the cavity frequency (the pulse frequency) and the $|2\rangle \leftrightarrow |3\rangle$ transition frequency of the transmon.

The infidelity mainly comes from the decoherence of the qutrits, the decay of the cavity, and the unwanted interactions caused by the pulse and the cavity, as well as the validity of the effective Hamiltonian in Eq. (9). To improve the fidelity, one can (i) employ a DRAG pulse [95,96] to reduce the leakage into the level $|2\rangle$, (ii) design the qutrits with larger level-spacing anharmonicity to reduce the effect of the unwanted interactions caused by the cavity, (iii) choose the qutrits with longer decoherence time and the cavity with a high quality factor, and (iv) optimize the ratio Δ/g to better meet the large detuning condition necessary for the effective Hamiltonian.

The operation time is ~ 0.45 μs, much shorter than the decoherence times of transmon qutrits used in our numerical simulations. For a transmon qutrit, the typical transition frequency between two adjacent levels is 1–20 GHz. As an example, consider $\omega_{10}/2\pi = 6.7$ GHz and $\omega_{21}/2\pi = 6.0$ GHz for the case of the transmon qutrits dispersively coupled to the cavity. With $\Delta/2\pi = 0.1$ GHz chosen above, we have $\omega_c = 5.9$ GHz. For $\kappa^{-1} = 10$ μs used in the numerical simulation, the cavity quality factor is $Q \sim 3.7 \times 10^5$, which is available because waveguide resonators with a (loaded) quality factor $Q \sim 10^6$ have been reported in experiments [97,98]. The analysis given here demonstrates that the high-fidelity creation of GHZ states of three logical qubits in a DFS is feasible with present circuit QED technology.

VII. CONCLUSION

We have presented an idea to realize quantum gates by manipulating quantum states outside the DFS but having the states of logical qubits stay in a DFS before and after the gate operation. This method has the following features. (i) Because the states are manipulated *outside* the DFS, the multiqubit gate implementation can be simplified when compared to realizing a multiqubit gate based on manipulating quantum states *within* the DFS, which usually requires unitary operations over a large DFS. (ii) Since the qubit states return to the DFS after the gate operation, decoherence during the state storage is avoided and the errors caused by decoherence during the gate operation are not accumulated for a long-running quantum computation. We should remark that, although the states of logical qubits are manipulated out of the DFS, the effect of decoherence from qubits during the gate operation can be made negligibly small as long as the operation time required for realizing a specific quantum gate is much shorter than the decoherence time of the qubits. This condition can be met by shortening the gate operation time or by choosing physical qubits with sufficient long energy relaxation time and dephasing time.

We have proposed a way for realizing a multi-target-qubit controlled-NOT gate using logical qubits encoded in a DFS against collective dephasing. This gate is realized by employing three-level qutrits placed in a cavity or coupled to a resonator. As shown above, our proposal of the gate implementation has the following advantages: (i) the states of the logical qubits return to the DFS after the gate operation, thus decoherence from qubits after the gate operation is avoided, (ii) the gate can be implemented with only a few basic operations, hence this proposal is quite simple, (iii) the gate operation time is independent of the number of logical qubits, (iv) the gate is implemented in a deterministic way because no measurement is used, (v) the intermediate level $|2\rangle$ for all qutrits is not occupied during the entire operation, thus decoherence from this level is avoided, and (vi) this proposal is universal and can be applied to realize the proposed gate using natural atoms or artificial atoms (e.g., quantum dots, NV centers, various superconducting qutrits, etc.) placed in a cavity or coupled to a resonator.

As an application, we have also shown how to apply this gate to create GHZ entangled states of multiple logical qubits encoded in a DFS. Our numerical simulations show that the high-fidelity creation of GHZ states of three logical qubits in a DFS is feasible within current circuit QED technology.

ACKNOWLEDGMENTS

This work is supported by the Key-Area Research and Development Program of GuangDong province (Grant No. 2018B030326001), the NKRDP of China (Grant No. 2016YFA0301802), and the National Natural Science Foundation of China (NSFC) (Grants No. 11074062, No. 11374083, and No. 11774076). This work is partially supported by MURI Center for Dynamic Magneto-Optics via the Air Force Office of Scientific Research (AFOSR) (Grant No. FA9550-14-1-0040), Army Research Office (ARO) (Grant No. W911NF18-1-0358), Japan Science and Technology Agency (JST) (via the Q-LEAP program and the CREST Grant No. JPMJCR1676), Japan Society for the Promotion of Science (JSPS) (JSPS-RFBR Grant No. 17-52-50023; JSPS-FWO Grant No. VS.059.18N), the RIKEN-AIST Challenge Research Fund, the Foundational Questions Institute (FQXi), and the NTT PHI Laboratory.

[1] A. Barenco, C. H. Bennett, R. Cleve, D. P. DiVincenzo, N. Margolus, P. Shor, T. Sleator, J. A. Smolin, and H. Weinfurter, Elementary gates for quantum computation, Phys. Rev. A **52**, 3457 (1995).

[2] M. Mötöen, J. J. Vartiainen, V. Bergholm, and M. M. Salomaa, Quantum Circuits for General Multiqubit Gates, Phys. Rev. Lett. **93**, 130502 (2004).

[3] V. V. Shende and I. L. Markov, On the CNOT-cost of TOFFOLI gates, Quantum Inf. Comput. **9**, 461 (2009).

[4] P. W. Shor, in *Proceedings of the 35th Annual Symposium on Foundations of Computer Science*, edited by S. Goldwasser (IEEE Computer Society, Los Alamitos, CA, 1994), pp. 124–134.

[5] L. K. Grover, Quantum Computers Can Search Rapidly by Using Almost Any Transformation, Phys. Rev. Lett. **80**, 4329 (1998).

[6] M. A. Nielsen and I. L. Chuang, *Quantum Computation and Quantum Information* (Cambridge University Press, Cambridge, England, 2001).

[7] P. W. Shor, Scheme for reducing decoherence in quantum computer memory, Phys. Rev. A **52**, R2493(R) (1995).

[8] A. M. Steane, Error Correcting Codes in Quantum Theory, Phys. Rev. Lett. **77**, 793 (1996).

[9] S. L. Braunstein, V. Bužek, and M. Hillery, Quantum information distributors: Quantum network for symmetric and asymmetric cloning in arbitrary dimension and continuous limit, Phys. Rev. A **63**, 052313 (2001).

[10] M. Šašura and V. Bužek, Multiparticle entanglement with quantum logic networks: Application to cold trapped ions, Phys. Rev. A **64**, 012305 (2001).

[11] M. Mariantoni, H. Wang, T. Yamamoto, M. Neeley, R. C. Bialczak, Y. Chen, M. Lenander, E. Lucero, A. D. O'Connell, D. Sank, M. Weides *et al.*, Implementing the quantum von Neumann architecture with superconducting circuits, Science **334**, 61 (2011).

[12] A. Fedorov, L. Steffen, M. Baur, M. P. daSilva, and A. Wallraff, Implementation of a Toffoli gate with superconducting circuits, Nature (London) **481**, 170 (2012).

[13] M. D. Reed, L. DiCarlo, S. E. Nigg, L. Sun, L. Frunzio, S. M. Girvin, and R. J. Schoelkopf, Realization of three-qubit quantum error correction with superconducting circuits, Nature (London) **482**, 382 (2012).

[14] X. Wang, A. Sørensen, and K. Mølmer, Multibit Gates for Quantum Computing, Phys. Rev. Lett. **86**, 3907 (2001).

[15] L. M. Duan, B. Wang, and H. J. Kimble, Robust quantum gates on neutral atoms with cavity-assisted photon-scattering, Phys. Rev. A **72**, 032333 (2005).

[16] C. P. Yang and S. Han, n-qubit-controlled phase gate with superconducting quantum-interference devices coupled to a resonator, Phys. Rev. A **72**, 032311 (2005).

[17] X. Zou, Y. Dong, and G. C. Guo, Implementing a conditional z gate by a combination of resonant interaction and quantum interference, Phys. Rev. A **74**, 032325 (2006).

[18] T. Monz, K. Kim, W. Häsel, M. Riebe, A. S. Villar, P. Schindler, M. Chwalla, M. Hennrich, and R. Blatt, Realization of the Quantum Toffoli Gate with Trapped Ions, Phys. Rev. Lett. **102**, 040501 (2009).

[19] S. Ashhab, P. C. de Groot, and F. Nori, Speed limits for quantum gates in multiqubit systems, Phys. Rev. A **85**, 052327 (2012).

[20] H. R. Wei and F. G. Deng, Universal quantum gates for hybrid systems assisted by quantum dots inside double-sided optical microcavities, Phys. Rev. A **87**, 022305 (2013).

[21] M. Hua, M. J. Tao, and F. G. Deng, Universal quantum gates on microwave photons assisted by circuit quantum electrodynamics, Phys. Rev. A **90**, 012328 (2014).

[22] B. Ye, Z. F. Zheng, and C. P. Yang, Multiplex-controlled phase gate with qubits distributed in a multicavity system, Phys. Rev. A **97**, 062336 (2018).

[23] C. P. Yang, Y. X. Liu, and F. Nori, Phase gate of one qubit simultaneously controlling n qubits in a cavity, Phys. Rev. A **81**, 062323 (2010).

[24] C. P. Yang, S. B. Zheng, and F. Nori, Multiqubit tunable phase gate of one qubit simultaneously controlling n qubits in a cavity, Phys. Rev. A **82**, 062326 (2010).

[25] C. P. Yang, Q. P. Su, F. Y. Zhang, and S. B. Zheng, Single-step implementation of a multiple-target-qubit controlled phase gate without need of classical pulses, Opt. Lett. **39**, 3312 (2014).

[26] H. F. Wang, A. D. Zhu, and S. Zhang, One-step implementation of a multiqubit phase gate with one control qubit and multiple target qubits in coupled cavities, Opt. Lett. **39**, 1489 (2014).

[27] T. Liu, X. Z. Cao, Q. P. Su, S. J. Xiong, and C. P. Yang, Multi-target-qubit unconventional geometric phase gate in a multicavity system, Sci. Rep. **6**, 21562 (2016).

[28] B. Ye, Z. F. Zheng, Y. Zhang, and C. P. Yang, Circuit QED: Single-step realization of a multiqubit controlled phase gate with one microwave photonic qubit simultaneously controlling $n-1$ microwave photonic qubits, Opt. Express **26**, 30689 (2018).

[29] Y. J. Fan, Z. F. Zheng, Y. Zhang, D. M. Lu, and C. P. Yang, One-step implementation of a multi-target-qubit controlled phase gate with cat-state qubits in circuit QED, Front. Phys. **14**, 21602 (2019).

[30] L. M. Duan and G. C. Guo, Preserving Coherence in Quantum Computation by Pairing Quantum Bits, Phys. Rev. Lett. **79**, 1953 (1997).

[31] P. Zanardi and M. Rasetti, Noiseless Quantum Codes, Phys. Rev. Lett. **79**, 3306 (1997).

[32] J. Q. You, X. Hu, and F. Nori, Correlation-induced suppression of decoherence in capacitively coupled Cooper-pair boxes, Phys. Rev. B **72**, 144529 (2005).

[33] P. G. Kwiat, A. J. Berglund, J. B. Altepeter, and A. G. White, Experimental verification of decoherence-free subspaces, Science **290**, 498 (2000).

[34] D. Kielpinski, V. Meyer, M. A. Rowe, C. A. Sackett, W. M. Itano, C. Monroe, and D. J. Wineland, A decoherence-free quantum memory using trapped ions, Science **291**, 1013 (2001).

[35] M. Mohseni, J. S. Lundeen, K. J. Resch, and A. M. Steinberg, Experimental Application of Decoherence-Free Subspaces in an Optical Quantum-Computing Algorithm, Phys. Rev. Lett. **91**, 187903 (2003).

[36] M. Bourennane, M. Eibl, S. Gaertner, C. Kurtsiefer, A. Cabello, and H. Weinfurter, Decoherence-Free Quantum Information Processing with Four-Photon Entangled States, Phys. Rev. Lett. **92**, 107901 (2004).

[37] L. A. Wu, P. Zanardi, and D. A. Lidar, Holonomic Quantum Computation in Decoherence-Free Subspaces, Phys. Rev. Lett. **95**, 130501 (2005).

[38] L. Aolita, L. Davidovich, K. Kim, and H. Häffner, Universal quantum computation in decoherence-free subspaces with hot trapped ions, Phys. Rev. A **75**, 052337 (2007).

[39] G. F. Xu, J. Zhang, D. M. Tong, and E. Sjöqvist, Nonadiabatic Holonomic Quantum Computation in Decoherence-Free Subspaces, Phys. Rev. Lett. **109**, 170501 (2012).

[40] S. B. Zheng, Universal quantum logic gates in decoherence-free subspace with atoms trapped in distant cavities, Sci. China Phys. Mech. Astron. **55**, 1571 (2012).

[41] Z. T. Liang, Y. X. Du, W. Huang, Z. Y. Xue, and H. Yan, Nonadiabatic holonomic quantum computation in decoherence-free subspaces with trapped ions, Phys. Rev. A **89**, 062312 (2014).

[42] G. Xu and G. Long, Universal nonadiabatic geometric gates in two-qubit decoherence-free subspaces, Sci. Rep. **4**, 6814 (2014).

[43] Z. Y. Xue, J. Zhou, and Z. D. Wang, Universal holonomic quantum gates in decoherence-free subspace on superconducting circuits, Phys. Rev. A **92**, 022320 (2015).

[44] V. Paulisch, H. J. Kimble, and A. González-Tudela, Universal quantum computation in waveguide QED using decoherence free subspaces, New J. Phys. **18**, 043041 (2016).

[45] Z. Zhu, T. Chen, X. Yang, J. Bian, Z. Y. Xue, and X. Peng, Single-Loop and Composite-Loop Realization of Nonadiabatic Holonomic Quantum Gates in a Decoherence-Free Subspace, Phys. Rev. Appl. **12**, 024024 (2019).

[46] B. Antonio and S. Bose, Two-qubit gates for decoherence-free qubits using a ring exchange interaction, Phys. Rev. A **88**, 042306 (2013).

[47] S. Hu, W. X. Cui, Qi. Guo, H. F. Wang, A. D. Zhu, and S. Zhang, Multi-qubit non-adiabatic holonomic controlled quantum gates in decoherence-free subspaces, Quantum Inf. Process. **15**, 3651 (2016).

[48] F. Nori, Quantum football, Science **325**, 689 (2009).

[49] M. Neeley, M. Ansmann, R. C. Bialczak, M. Hofheinz, N. Katz, E. Lucero, A. O'Connell, H. Wang, A. N. Cleland, and J. M. Martinis, Process tomography of quantum memory in a Josephson-phase qubit coupled to a two-level state, Nat. Phys. **4**, 523 (2008).

[50] A. Miranowicz, M. Paprzycka, A. Pathak, and F. Nori, Phase-space interference of states optically truncated by quantum scissors: Generation of distinct superpositions of qudit coherent states by displacement of vacuum, Phys. Rev. A **89**, 033812 (2014).

[51] Y. Han, X. Q. Luo, T. F. Li, W. Zhang, S. P. Wang, J. S. Tsai, F. Nori, and J. Q. You, Time-Domain Grating with a Periodically Driven Qutrit, Phys. Rev. Appl. **11**, 014053 (2019).

[52] P. Pradhan, M. P. Anantram, and K. L. Wang, Quantum computation by optically coupled steady atoms/quantum-dots inside a quantum electro-dynamic cavity, arXiv:quant-ph/0002006.

[53] P. Neumann, R. Kolesov, V. Jacques, J. Beck, J. Tisler, A. Batalov, L. Rogers, N. B. Manson, G. Balasubramanian, and F. Jelezko, Excited-state spectroscopy of single NV defects in diamond using optically detected magnetic resonance, New J. Phys. **11**, 013017 (2009).

[54] P. J. Leek, S. Filipp, P. Maurer, M. Baur, R. Bianchetti, J. M. Fink, M. Goppl, L. Steffen, and A. Wallraff, Using sideband transitions for two-qubit operations in superconducting circuits, Phys. Rev. B **79**, 180511 (2009).

[55] M. Brune, E. Hagley, J. Dreyer, X. Maitre, A. Maali, C. Wunderlich, J. M. Raimond, and S. Haroche, Observing the Progressive Decoherence of the "Meter" in a Quantum Measurement, Phys. Rev. Lett. **77**, 4887 (1996).

[56] M. Sandberg, C. M. Wilson, F. Persson, T. Bauch, G. Johansson, V. Shumeiko, T. Duty, and P. Delsing, Tuning the field in a microwave resonator faster than the photon lifetime, Appl. Phys. Lett. **92**, 203501 (2008).

[57] Z. L. Wang, Y. P. Zhong, L. J. He, H. Wang, J. M. Martinis, A. N. Cleland, and Q. W. Xie, Quantum state characterization of a fast tunable superconducting resonator, Appl. Phys. Lett. **102**, 163503 (2013).

[58] S. B. Zheng and G. C. Guo, Efficient Scheme for Two-Atom Entanglement and Quantum Information Processing in Cavity QED, Phys. Rev. Lett. **85**, 2392 (2000).

[59] D. F. V. James and J. Jerke, Effective Hamiltonian theory and its applications in quantum information, Can. J. Phys. **85**, 625 (2007).

[60] T. Monz, P. Schindler, J. T. Barreiro, M. Chwalla, D. Nigg, W. A. Coish, M. Harlander, W. Hansel, M. Hennrich, and R. Blatt, 14-Qubit Entanglement: Creation and Coherence, Phys. Rev. Lett. **106**, 130506 (2011).

[61] C. Song, K. Xu, W. Liu, C. P. Yang, S. B. Zheng, H. Deng, Q. Xie, K. Huang, Q. Guo, L. Zhang *et al.*, 10-Qubit Entanglement and Parallel Logic Operations with a Superconducting Circuit, Phys. Rev. Lett. **119**, 180511 (2017).

[62] X. L. Wang, Y. H. Luo, H. L. Huang, M. C. Chen, Z. E. Su, C. Liu, C. Chen, W. Li, Y. Q. Fang, X. Jiang *et al.*, 18-Qubit Entanglement with Six Photons' Three Degrees of Freedom, Phys. Rev. Lett. **120**, 260502 (2018).

[63] H. S. Zhong, Y. Li, W. Li, L. C. Peng, Z. E. Su, Y. Hu, Y. M. He, X. Ding, W. Zhang, H. Li *et al.*, 12-Photon Entanglement and Scalable Scattershot Boson Sampling with Optimal Entangled-Photon Pairs from Parametric Down-Conversion, Phys. Rev. Lett. **121**, 250505 (2018).

[64] A. Omran, H. Levine, A. Keesling, G. Semeghini, T. T. Wang, S. Ebadi, H. Bernien, A. S. Zibrov, H. Pichler, S. Choi *et al.*, Generation and manipulation of Schrödinger cat states in Rydberg atom arrays, Science **365**, 570 (2019).

[65] C. Song, K. Xu, H. Li, Y. Zhang, X. Zhang, W. Liu, Q. Guo, Z. Wang, W. Ren, J. Hao, H. Feng, H. Fan, D. Zheng, D. Wang, H. Wang, and S. Zhu, Observation of multi-component atomic Schrödinger cat states of up to 20 qubits, Science **365**, 574 (2019).

[66] C. C. Gerry, Preparation of multiatom entangled states through dispersive atom–cavity-field interactions, Phys. Rev. A **53**, 2857 (1996).

[67] S. B. Zheng, One-Step Synthesis of Multiatom Greenberger-Horne-Zeilinger States, Phys. Rev. Lett. **87**, 230404 (2001).

[68] L. M. Duan and H. Kimble, Efficient Engineering of Multiatom Entanglement through Single-Photon Detections, Phys. Rev. Lett. **90**, 253601 (2003).

[69] X. Wang, M. Feng, and B. C. Sanders, Multipartite entangled states in coupled quantum dots and cavity QED, Phys. Rev. A **67**, 022302 (2003).

[70] S. L. Zhu, Z. D. Wang, and P. Zanardi, Geometric Quantum Computation and Multiqubit Entanglement with Superconducting Qubits Inside a Cavity, Phys. Rev. Lett. **94**, 100502 (2005).

[71] S. Matsuo, S. Ashhab, T. Fujii, F. Nori, K. Nagai, and N. Hatakenaka, in *Generation of Bell States and Greenberger–Horne–Zeilinger States in Superconducting Phase Qubits, Quantum Communication, Measurement and Computing*, edited by O. Hirota *et al.* (NICT, Tokyo, 2006), No. 8.

[72] L. F. Wei, Y. X. Liu, and F. Nori, Generation and Control of Greenberger-Horne-Zeilinger Entanglement in Superconducting Circuits, Phys. Rev. Lett. **96**, 246803 (2006).

[73] S. Matsuo, S. Ashhab, T. Fujii, F. Nori, K. Nagai, and N. Hatakenaka, Generation of macroscopic entangled states in coupled superconducting phase qubits, J. Phys. Soc. Jpn. **76**, 054802 (2007).

[74] S. Aldana, Y. D. Wang, and C. Bruder, Greenberger-Horne-Zeilinger generation protocol for N superconducting transmon qubits capacitively coupled to a quantum bus, Phys. Rev. B **84**, 134519 (2011).

[75] P. B. Li and F. L. Li, Deterministic generation of multiparticle entanglement in a coupled cavity-fiber system, Opt. Express **19**, 1207 (2011).

[76] C. P. Yang, Q. P. Su, S. B. Zheng, and F. Nori, Entangling superconducting qubits in a multi-cavity system, New J. Phys. **18**, 013025 (2016).

[77] X. B. Huang, Y. H. Chen, and Z. Wang, Fast generation of three-qubit Greenberger-Horne-Zeilinger state based on the Lewis-Riesenfeld invariants in coupled cavities, Sci Rep. **6**, 25707 (2016).

[78] M. Izadyari, M. Saadati-Niari, R. Khadem-Hosseini, and M. Amniat-Talab, Creation of N-atom GHZ state in atom-cavity-fiber system by multi-state adiabatic passage, Opt. Quantum Electron. **48**, 71 (2016).

[79] Y. Zhou, B. Li, X. X. Li, F. L. Li, and P. B. Li, Preparing multiparticle entangled states of NV centers via adiabatic ground-state transitions, Phys. Rev. A **98**, 052346 (2018).

[80] X. T. Mo and Z. Y. Xue, Single-step multipartite entangled states generation from coupled circuit cavities, Front. Phys. **14**, 31602 (2019).

[81] J. Q. You and F. Nori, Superconducting circuits and quantum information, Phys. Today **58**(11), 42 (2005).

[82] J. Clarke and F. K. Wilhelm, Superconducting quantum bits, Nature (London) **453**, 1031 (2008).

[83] J. Q. You and F. Nori, Atomic physics and quantum optics using superconducting circuits, Nature (London) **474**, 589 (2011).

[84] I. Buluta, S. Ashhab, and F. Nori, Natural and artificial atoms for quantum computation, Rep. Prog. Phys. **74**, 104401 (2011).

[85] Z. L. Xiang, S. Ashhab, J. Q. You, and F. Nori, Hybrid quantum circuits: Superconducting circuits interacting with other quantum systems, Rev. Mod. Phys. **85**, 623 (2013).

[86] X. Gu, A. F. Kockum, A. Miranowicz, Y. X. Liu, and F. Nori, Microwave photonics with superconducting quantum circuits, Phys. Rep. **718–719**, 1 (2017).

[87] A. F. Kockum and F. Nori, Quantum bits with Josephson junctions, in *Fundamentals and Frontiers of the Josephson Effect*, edited by F. Tafuri, Springer Series in Materials Science Vol. 286 (Springer, Berlin, 2019), Chap. 17, pp. 703–741.

[88] J. Koch, T. M. Yu, J. Gambetta, A. A. Houck, D. I. Schuster, J. Majer, A. Blais, M. H. Devoret, S. M. Girvin, and R. J. Schoelkopf, Charge-insensitive qubit design derived from the Cooper pair box, Phys. Rev. A **76**, 042319 (2007).

[89] J. Q. You, X. Hu, S. Ashhab, and F. Nori, Low-decoherence flux qubit, Phys. Rev. B **75**, 140515(R) (2007).

[90] I. C. Hoi, C. M. Wilson, G. Johansson, T. Palomaki, B. Peropadre, and P. Delsing, Demonstration of a Single-Photon Router in the Microwave Regime, Phys. Rev. Lett. **107**, 073601 (2011).

[91] For a transmon qutrit, the $|0\rangle \leftrightarrow |2\rangle$ transition is much weaker than those of the $|0\rangle \leftrightarrow |1\rangle$ and $|1\rangle \leftrightarrow |2\rangle$ transitions. Thus we have $\gamma_{20}^{-1} \gg \gamma_{10}^{-1}, \gamma_{21}^{-1}$.

[92] M. J. Peterer, S. J. Bader, X. Jin, F. Yan, A. Kamal, T. J. Gudmundsen, P. J. Leek, T. P. Orlando, W. D. Oliver, and S. Gustavsson, Coherence and Decay of Higher Energy Levels of a Superconducting Transmon Qubit, Phys. Rev. Lett. **114**, 010501 (2015).

[93] C. Wang, Y. Y. Gao, P. Reinhold, R. W. Heeres, N. Ofek, K. Chou, C. Axline, M. Reagor, J. Blumoff, K. M. Sliwa,

L. Frunzio, S. M. Girvin, L. Jiang, M. Mirrahimi, M. H. Devoret, and R. J. Schoelkopf, A Schrödinger cat living in two boxes, Science **352**, 1087 (2016).

[94] M. Baur, A. Fedorov, L. Steffen, S. Filipp, M. P. da Silva, and A. Wallraff, Benchmarking a Quantum Teleportation Protocol in Superconducting Circuits Using Tomography and an Entanglement Witness, Phys. Rev. Lett. **108**, 040502 (2012).

[95] F. Motzoi, J. M. Gambetta, P. Rebentrost, and F. K. Wilhelm, Simple Pulses for Elimination of Leakage in Weakly Nonlinear Qubits, Phys. Rev. Lett. **103**, 110501 (2009).

[96] J. M. Gambetta, F. Motzoi, S. T. Merkel, and F. K. Wilhelm, Analytic control methods for high-fidelity unitary operations in a weakly nonlinear oscillator, Phys. Rev. A **83**, 012308 (2011).

[97] W. Chen, D. A. Bennett, V. Patel, and J. E. Lukens, Substrate and process dependent losses in superconducting thin film resonators, Supercond. Sci. Technol. **21**, 075013 (2008).

[98] P. J. Leek, M. Baur, J. M. Fink, R. Bianchetti, L. Steffen, S. Filipp, and A. Wallraff, Cavity Quantum Electrodynamics with Separate Photon Storage and Qubit Readout Modes, Phys. Rev. Lett. **104**, 100504 (2010).